

T-type calcium channel blockade induces apoptosis in C2C12 myotubes and skeletal muscle via endoplasmic reticulum stress activation

Mao Chen, Suting Li, Menglei Hao, Jue Chen, Zhihan Zhao, Shasha Hong, Jie Min, Jianming Tang, Ming Hu and Li Hong 

Department of Gynecology and Obstetrics, Renmin Hospital of Wuhan University, China

Keywords

apoptosis; endoplasmic reticulum stress; skeletal muscle wasting; T-type calcium channel

Correspondence

L. Hong, Department of Gynecology and Obstetrics, Renmin Hospital of Wuhan University, #238 Jiefang Road, Wuhan, Hubei 430060, China
Tel: +86 027-88041911-82289
E-mail: dr_hongli@whu.edu.cn

(Received 17 June 2020, revised 11 August 2020, accepted 25 August 2020)

doi:10.1002/2211-5463.12965

Loss of T-type calcium channel (TCC) function has been reported to result in decreased cell viability and impaired muscle regeneration, but the underlying mechanisms remain largely unknown. We previously found that expression of TCC is reduced in aged pelvic floor muscle of multiple vaginal delivery mice, and this is related to endoplasmic reticulum stress (ERS) activation and autophagy flux blockade. In the present work, we further investigated the effects of TCC function loss on C2C12 myotubes and skeletal muscle, which is mediated by promotion of ERS and ultimately contributes to mitochondrial-related apoptotic cell death. We found that application of a TCC inhibitor induced mitochondria-related apoptosis in a dose-dependent manner and also reduced mitochondrial transmembrane potential (MMP), induced mito-ROS generation, and enhanced expression of mitochondrial apoptosis proteins. Functional inhibition of TCC induced ERS, resulting in disorder of Ca^{2+} homeostasis in endoplasmic reticulum, and ultimately leading to cell apoptosis in C2C12 myotubes. Tibialis anterior muscles of T-type $\alpha 1\text{H}$ channel knockout mice displayed a smaller skeletal muscle fiber size and elevated ERS-mediated apoptosis signaling. Our data point to a novel mechanism whereby TCC blockade leads to ERS activation and terminal mitochondrial-related apoptotic events in C2C12 myotubes and skeletal muscles.

Skeletal muscle represents approximately 50–75% of the total body's proteins and is a highly dynamic and plastic organ that is responsible for generating the force [1]. Muscle wasting occurs systemically in many diseases conditions, including sarcopenia, cancer-associated cachexia, sepsis, burns, and trauma [2]. Accumulating evidence indicates that the loss of skeletal muscle mass is associated with excessive apoptosis caused by a wide array of environmental and genetic factors [3–5]. However, its pathogenesis remains largely unclear.

Skeletal muscle contains a complicated network of the endoplasmic reticulum (ER) called the sarcoplasmic reticulum (SR), which is arranged in a dynamic tubular network. The ER is primarily recognized as the site of synthesis and folding of secreted proteins, serving as the site of Ca^{2+} uptake, storage, and release, which plays an important role in the regulation of proteostasis and calcium homeostasis in sophisticated scenarios [6,7]. Altered ER homeostasis leads to the accumulation of unfolded or misfolded proteins in the

Abbreviations

4-PBA, 4-phenylbutyrate; CHOP, C/EBP-homologous protein; CSA, cross-sectional area; DM, differentiation medium; ER, endoplasmic reticulum; ERS, endoplasmic reticulum stress; GRP78, glucose-regulated protein 78; MMP, mitochondria transmembrane potential; NNC-55, NNC 55-0396 hydrate; SR, sarcoplasmic reticulum; TA, tibialis anterior; TCC, T-type calcium channel; TH, T-type $\alpha 1\text{H}$ channel; THKO, T-type $\alpha 1\text{H}$ channel knockout; ThT, thioflavin T; TUDAC, tauroursodeoxycholic acid.

ER lumen that may activate a homeostatic signaling network termed ER stress (ERS) [8]. ERS is buffered by activation of the unfolded protein response (UPR), which is initiated by three pivotal stress sensors [8,9]. All three ERS sensors are maintained in an inactive state through their association with the ER chaperone glucose-regulated protein 78 (GRP78) in resting cells and are activated by its dissociation [10]. Specific transcription factors are then activated, triggering the expression of UPR-related genes [such as the proapoptotic transcription factor C/EBP-homologous protein (CHOP)] [11,12]. The role of CHOP in ERS-induced apoptosis has been illustrated in *Chop*^{-/-} mice [13]. Moreover, the activation of ERS signal cascades has been observed in skeletal muscle in multiple muscle-wasting disease conditions with GRP78 upregulated [14,15].

Emerging clinical, histopathological, and electrophysiological evidences suggest that alteration of T-type Ca²⁺ channel (TCC) activity is likely to affect muscle afferent signaling and may be associated with amyotrophy and apoptosis sensitivity [16,17]. There are three subtypes of TCC, and the T-type $\alpha 1H$ channel (TH) is the most significantly expressed [18]. A recent clinical study identified a loss-of-TH channel function because of *CACNA1H* variants is associated with infantile-onset amyotrophy, perhaps through dysfunctional Ca²⁺ signaling [16]. Otherwise, the amplitude of T-type Ca²⁺ currents has been found decreased significantly in aged skeletal muscle and aged satellite cells (SCs), resulting in inefficiency and the inability to fuse into myotubes during myogenic differentiation due to defective T-type Ca²⁺ currents [19]. These results indicate that the function loss of TCC may play an important role in the pathogenesis of muscle wasting. On the basis of these studies, one new finding of cardiovascular diseases confirmed that both siRNA-mediated gene knockdown and TCC blockers can induce ERS with relevance to cell viability [17]. Apart from the well-established role of TCC blockade in cancer, cardiovascular diseases, and neurological disorders [20–23], the consequences of TCC defects in skeletal muscle are still unknown.

We previously identified that the expression of TH (*CACNA1H*) is higher than that of the other two types in mammalian skeletal muscle and myoblasts. TCC inhibition by NNC 55-0396 hydrate (NNC-55) promoted ERS activation and autophagosome formation but blocked distal autophagy and autophagy flux [24]. Given that ERS is upstream of autophagy blockade induced by NNC-55 and mitochondrial dysfunction could regulate autophagic process through ROS production and mitochondria-specific proteins [25], we

explore the primary effects of TCC function loss on ERS activation and mitochondrial-related apoptosis. In this study, we found TCC inhibition induced ER-Ca²⁺ disorder and ERS activation, which contributed to mitochondrial-related apoptosis.

Material and methods

Cell culture and study design

C2C12 myoblasts were purchased from Cbioer Biosciences Co., Ltd. (Nanjing, China) and maintained in growth medium [Dulbecco's Modified Eagle Medium (DMEM) with 10% fetal bovine serum and 1% penicillin–streptomycin] in 5% CO₂ at 37 °C for proliferation. For myogenesis, C2C12 myoblasts cultured in 6-well plates were transferred into differentiation medium (DM; containing DMEM and 2% horse serum, 1% penicillin–streptomycin) for 4 days after reaching 80–90% confluence. The C2C12 myotubes were then treated with different drug interventions, respectively, for 24 h in DM for related analysis.

NNC-55 (Sigma-Aldrich Co, St. Louis, MO, USA), ERS inhibitors including sodium 4-phenylbutyrate (4PBA, No.1716-12-7; MedChemExpress, Monmouth Junction, NJ, USA) and tauroursodeoxycholic acid (TUDAC, CAS No.35807-85-3, MedChemExpress), and intracellular Ca²⁺ chelator of BAPTA-AM (CAS No.126150-97-8; MedChemExpress) were all dissolved in DMSO (Sigma-Aldrich) and stored at –20 °C or –80 °C.

For transfection, C2C12 myoblasts were transfected with negative-control siRNA (NC) and three small interfering RNAs against TH including siRNA-1, 2 and 3 (si-1/si-m-Cacna1h-001 5'-GGGTAAACATCATGTACGA-3', si-2/si-m-Cacna1h-002 5'-GGAATGTGGTTCTTTACAA-3' and si-3/si-m-Cacna1h-003 5'-GTCGCATTGTAGACAGCA-3', Ribobio, Guangzhou, China) using riboFECT™CP Transfection Kit at a final concentration of 50 nM according to the manufacturer's protocol. After 48-h transduction, the efficiency of TH knockdown was verified by quantitative real-time PCR (qRT-PCR), and the cells were cultured in DM for another 4 days to fuse into myotubes for subsequent analysis.

Animals' management and sample

All experimental protocols of the animal study described here were approved by the Institutional Animal Care and Ethics Committee of the Renmin Hospital of Wuhan University (2016-1105). All animal experiments comply with the ARRIVE guidelines and were carried out in accordance with the National Institutes of Health guide for the care and use of Laboratory animals. The TH knockout (THKO) mice were obtained from Jackson Laboratory (stock number 013770), and 4-month-old female mice were

used for this experiment ($n = 7$). Female C57BL/6 mice, 4 months old, were obtained from the Experimental Animal Center of the Renmin Hospital of Wuhan University and used for a control group ($n = 7$). All mice were housed in a pathogen-free barrier facility and were placed on a standard chow, *ad libitum*, in a temperature-controlled room (21–22 °C) on a 12-h light cycle for a week. All mice were sacrificed by cervical dislocation, and the left tibialis anterior (TA) muscles were harvested and fixed in 4% paraformaldehyde overnight, embedded in paraffin, and sectioned into muscle tissue sections, while right TA muscles preserved in -80 °C.

Nuclear staining with Hoechst 333258

C2C12 myotubes that seeded onto glass coverslips in six-well culture plate were fixed with 4% paraformaldehyde in PBS (Genom Biotech Ltd., Hangzhou, China) for 30 min and stained with Hoechst 333258 (Beyotime, China) for 20 min at room temperature. Then, cells were washed with PBS three times and examined under a fluorescence microscope (Olympus, Tokyo, Japan).

Assays for mitochondria transmembrane potential by JC-1 staining

The decrease of mitochondrial membrane potential is an iconic event in the early stages of apoptosis. The mitochondria with a lower membrane potential ($\Delta\Psi_m$) can be easily detected by the transformation of JC-1 from red fluorescence (J-aggregates) to green fluorescence (monomer). The mitochondrial transmembrane potential was assessed with a Mitochondrial Membrane Potential Assay Kit (Beyotime), termed JC-1 staining, according to the manufacturer's instructions. Briefly, add the CCCP (10 mM) recommended in the kit to the cell culture medium for 20 min as a positive control group. The indicated cells were loaded with $1 \times$ JC-1 staining solution at 37 °C in the dark for 20 min and then washed, and a total of 20 000-gated events analyzed by a flow cytometer (BD Biosciences, Franklin Lakes, NJ, USA). The JC-1 fluorescence of red: green ratio was determined. The experiment was performed in triplicate.

Mitochondrial superoxide production

Mitochondrial reactive oxygen species (mito-ROS) production was measured using the MitoSOX™ Red mitochondrial superoxide indicator (40778ES50; Yeasen Biotech Co., Ltd., Shanghai, China) according to the manufacturer's instructions. DAPI was used as an indicator of nuclei. Cells were incubated with $5 \mu\text{M}$ MitoSOX™ Red solution for 15 min, washed three times, and mounted with DAPI, and images were then captured with a fluorescence microscope. Fluorescent intensity was analyzed by IMAGEJ analysis

software (National Institutes of Health, Bethesda, MD, USA). In each experiment, more than 100 cells were investigated. The experiments were repeated three times.

Intracellular Ca^{2+} detection in single C2C12 cell

The intracellular Ca^{2+} levels were measured using $10 \mu\text{M}$ Fluo-3 AM (Sigma-Aldrich). The treated and control cells were washed with Ca^{2+} -free Hank's balanced salt solution (HBSS, without phenolsulfonphthalein; Procell Life Science & Technology Co., Ltd., Wuhan, China) three times. After incubation with Fluo-3 MA for 30 min at 37 °C with 5% CO_2 , cells were washed with HBSS three times. The fluorescence signals were detected in DM with a confocal laser scanning system (FV1200; Olympus Corp) by an argon laser at 488 nm and emitted a fluorescence beam at 530 nm, scanning the XY plane using the Times Course program. Images were acquired by continuous scanning to observe the fluorescence intensity changes of Ca^{2+} in each group, which was automatically plotted by LSCM image analysis system. Low concentration of KCl evoked increases of intracellular Ca^{2+} concentration by inducing Ca^{2+} influx. To estimate basal Ca^{2+} level, the average Ca^{2+} value for 1 min before stimulation was used. The increment of Ca^{2+} was calculated by subtraction of the basal level from each stimulus-induced peak Ca^{2+} level (30 mM KCl). To quantify the effect of NNC-55, basal Ca^{2+} level at rest and relative amplitude of Ca^{2+} induced by 30 mM KCl were calculated.

Dye binding assays for ThT assay

Thioflavin T (ThT) is known to be able to detect ERS by exhibiting fluorescence when it binds to protein aggregates according to Beriault and Werstuck [26]. Briefly, cells were fixed in 4% paraformaldehyde, permeabilized by 0.1% Triton X/PBS, washed 3 times, and incubated with ThT (MedChemExpress) at the final concentration of $5 \mu\text{M}$ for 20 min at 37 °C. After washing three times with PBS, we mounted to slides using two drops of Fluoromount and stored at 4 °C in the dark. Confocal images were captured using an automatic microscope (BX63, Olympus Corp).

Transmission electron microscopy analysis

Tibialis anterior muscles or cells were fixed in 2% glutaraldehyde (Servicebio, Inc., Wuhan, China) for 2 h. After a thorough rinsing in PBS, samples were post-fixed in 1% osmium tetroxide and subsequently dehydrated with a graded series of ethanol. Samples were then embedded in Epon Resin 618. Ultrathin sections were obtained with a microtome, stained with uranyl acetate and lead citrate. Alterations in ER/SR and mitochondrial morphology were

imaged using a Hitachi transmission electron microscope (HT7700; Hitachi, Ltd., Tokyo, Japan).

Quantitative real-time PCR

Total RNA was extracted from subjected cells using TRIzol reagent (Takara Bio Inc., Otsu, Japan) and then reverse-transcribed into cDNA using the HifairTM II 1st Strand cDNA Synthesis Super Mix (gDNA digester plus; Yeasen Biotech Co., Ltd.). The primers for SERCA1, RyR1, IP3R1, GRP78, and CHOP were obtained from Yeasen Biotech Co., Ltd.. Primer sequences are listed in Table 1. The HieffTM qPCR SYBR[®] Green Master Mix (NO Rox Plus; Yeasen Biotech Co., Ltd.) reagent was used for qRT-PCR, and the CFX96 Trademark Real-time PCR detection system (Bio-Rad, California, USA) was used for analysis. PCR thermal cycling conditions were 95 °C for 5 min, which could activate DNA polymerase, followed by 40 cycles (95 °C for 10 s, 56 °C for 20 s, and 72 °C for 20 s). Each experiment was performed in triplicates and repeated at least three times. The data of relative mRNA levels were calculated by the $2^{-\Delta\Delta Cq}$ method, and results were normalized to GAPDH expression and relative to expression in control.

Immunofluorescence analysis

Immunofluorescent staining was performed for laminin (to demarcate the muscle fiber boundaries) and DAPI (to label the nuclei) co-stained muscle images, and thus, muscle fiber size distribution can be plotted and analyzed by cross-sectional area (CSA). Paraffin-embedded TA muscle tissue sections were dewaxed by heating at 60 °C and washing in xylene (Sinopharm Chemical Reagent Co., Ltd., Shanghai, China) and rehydrated with a graded series of ethanol. Then, antigen retrieval was performed with microwave or citrate antigen retrieval solution followed by two washes with PBS and 1-h incubation with blocking solution (5% BSA) prior to overnight incubation at 4 °C with rabbit polyclonal anti-laminin primary antibody at 1 : 100 (Abcam, Cambridge, UK). Then, the tissue sections were incubated with the secondary antibody (Maxim Biotechnologies, Shanghai, China) labeled with FITC for 1 h at room temperature after washing extensively three times

with PBS. Finally, the sections were mounted with DAPI and imaged with fluorescence microscope. Images were analyzed by ImageJ software (NIH, Bethesda, MD, USA).

TUNEL analysis

Paraffin-embedded sections of 5- μ m thickness were dewaxed by heating at 60 °C and washing in xylene (Sinopharm Chemical Reagent Co., Ltd.) and rehydrated with a graded series of ethanol. Then, in order to investigate apoptosis, terminal deoxynucleotidyl transferase-mediated dUTP nick end labeling (TUNEL) analysis was performed on the muscle tissue sections using a commercially available TUNEL assay kit, in situ Cell Death Detection Kit, Fluorescein (Roche Diagnostics GmbH, Mannheim, Germany), following the manufacturer's protocol. The sections were incubated with a protease K working solution for 20 min at room temperature and then incubated with permeabilization solution for 10 min. After washing extensively three times with PBS, they were incubated with the TUNEL reaction mixture for 60 min at 37 °C in the dark. Finally, the sections were washed three times in PBS and imaged with fluorescence microscopy (IX51). The number of apoptotic cells and the total number of cells were calculated respectively.

Western blot analysis

Tissue and cell extracts were homogenized in RIPA Lysis Buffer containing phenylmethylsulfonyl fluoride, centrifuged, and collected the supernatant to obtain whole cell lysates, and protein concentration was determined with the same way. Equal amounts of protein extracts were denatured by boiling at 100 °C for 8 min in SDS/PAGE Sample Loading Buffer. Next, the proteins were separated by 12% SDS/PAGE and then transferred to poly(vinylidene difluoride) membranes, blocked with 5% nonfat milk in Tris-buffered saline with 0.05% Tween-20 buffer (TBST) for 1 h at room temperature and incubated overnight at 4 °C with the following primary antibodies: rabbit antibodies against Bax (1 : 1000; Cell Signaling Technology Inc., Danvers, MA, USA), cleaved-caspase3 (1 : 1000; Absin Bioscience Inc., Shanghai, China), Cytochrome c (Cyt-c, 1 : 1000; Proteintech Group, Inc., Chicago, IL, USA), CHOP (1 : 1000 Proteintech Group, Inc.), Bcl2 (1 : 1000

Table 1. Primers for qRT-PCR.

Gene	Forward primer(5'-3')	Reverse primer(5'-3')
SERCA1	5'-CTCACACAAGTCCAAGATTGTG-3'	5'-GAGAAGTTATCATCGGCCAGTA-3'
RyR1	5'-CTGGGCTATGGCTACAACATC-3'	5'-GACTGCTTCAAACCTCGAAGTAC-3'
IP3R1	5'-GTTTGAGAAATTCCTCGTGGAC-3'	5'-CATCACGATTTTCAGTGACGTAC-3'
GRP78	5'-ATGATGAAGTTCAGTGTGGTGG-3'	5'-CTGATCGTTGGCTATGATCTCC-3'
CHOP	5'-CTCCAGATTCAGTCAGAGTTC-3'	5'-ACTCTGTTTCCGTTTCCCTAGTT-3'

Proteintech Group, Inc.), cleaved-caspase 9 (1 : 1000; Cell Signaling Technology Inc.), β -actin (1 : 3000; Proteintech Group, Inc.), and GRP78/BIP (1 : 3000; Proteintech Group, Inc.). The blots were washed with TBS-T buffer three times and then incubated with horseradish peroxidase-labeled goat anti-rabbit IgG (H + L) secondary antibodies (1 : 3000; Servicebio, Inc.) for 1 h at room temperature. After washing with TBST, the blots were visualized using BeyoECL Star (Beyotime) and quantified using the Molecular Imager ChemiDoc Touch Imaging System with Image Lab 5.2 quantitative assay system (Bio-Rad Laboratories, Inc., Hercules, CA, USA). The β -actin protein was used as a control.

Statistical analysis

All experimental data points are independent, and data are presented as the mean \pm SD. Statistical software spss 17.0 (SPSS Inc., Chicago, IL, USA) was used for statistical analysis. For normally distributed data, one-way analysis of variance (ANOVA) was used for multiple comparisons and Dunnett's test for comparing each group with the control group. Student's *t*-tests (unpaired two-tailed) were applied for comparing two groups. $P < 0.05$ was considered to indicate a statistically significant difference.

Results

TCC inhibition promotes apoptosis in C2C12 myotubes in a dose-dependent manner

The morphology of NNC-55-treated C2C12 cells showed increased surface blebs, a cytological feature of C2C12 myotube apoptosis [27], and decreased myotube formation, which positively correlated with the concentration of NNC-55 (Fig. 1A). This was further confirmed by analyzing the nuclear morphology that the apoptotic cells with strong fluorescence, fragmented, or condensed nuclei were observed under fluorescent microscopy, which showed that apoptosis increased in the same dose-dependent manner (Fig. 1B). Similar results revealed that NNC-55 treatment significantly reduced mitochondria transmembrane potential (MMP), increased mitochondria-derived ROS levels, and expression of apoptotic protein (Cyt-c, Bax upregulated, and Bcl2 downregulated) in myotubes (Fig. 1C–H), which are suggestive of apoptosis induction. These results suggested that pharmacological inhibition of TCC promoted apoptosis of C2C12 myotubes in a dose-dependent manner.

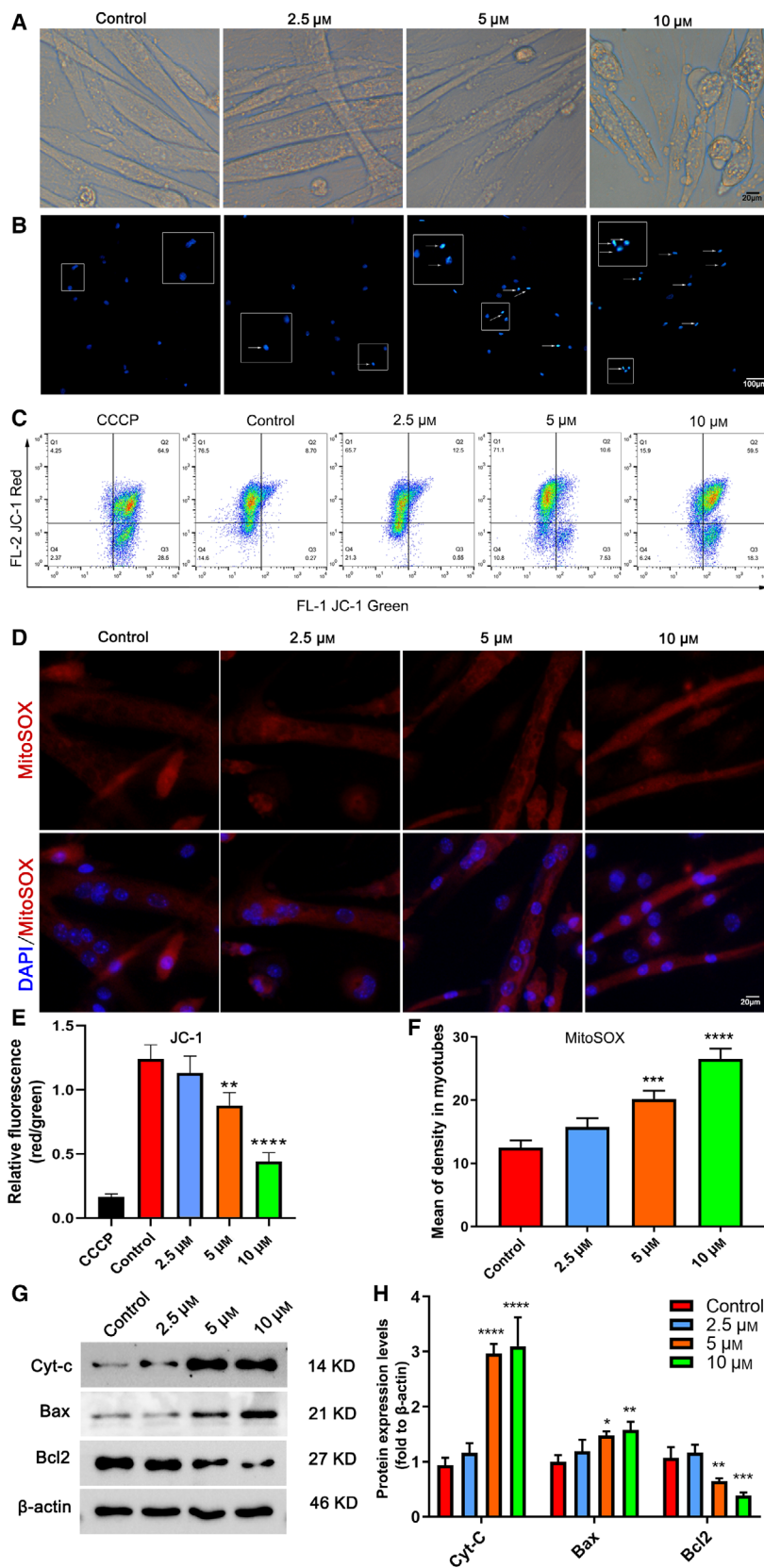
TCC inhibition increases ER-Ca²⁺ release and interferes with ER Ca²⁺ homeostasis

Considering that apoptosis induction is associated with elevated intracellular Ca²⁺, a possible explanation for

why C2C12 myotubes apoptosis increased after TCC inhibitor treatment may be pharmacological inhibitor-mediated reduction in ER-Ca²⁺ storage levels [28]. We examined the changes in intracellular Ca²⁺ levels after NNC-55 treatment for 24 h using the fluorescent dye Fluo-3 AM. It is known that low concentration of KCl evoked increases of intracellular Ca²⁺ concentration by inducing Ca²⁺ influx. We found intracellular Ca²⁺ started to increase after stimulation with 15 mM KCl and then peaked at 30 mM in C2C12 myotubes (data not shown), consistent with previous research [29]. As shown in Fig. 2A, the level of intracellular basal Ca²⁺ at rest was elevated, but the Ca²⁺ influx into cell at peak-rest induced by 30 mM KCl in NNC-55-treated myotubes was less than that in control cells. These data indicated that the increased intracellular Ca²⁺ level is not due to the influx of extracellular Ca²⁺. Consequently, the mRNAs levels related to important molecular components of the Ca²⁺ handling machinery in the ER were upregulated. The results revealed that NNC-55 treatment for 24 h increased ER-Ca²⁺ release and induced dysregulation of ER-Ca²⁺ homeostasis, as indicated by upregulated expression of SERCA1, RYR1, and IP3R1 (Fig. 2B). We also observed morphological changes in ER under transmission electron microscopy. Compared to the ER of the control, which had no swelling or expansion, the ER of the NNC-55 group showed more edema, expansion, and vacuolation of the cavity and degranulation as noted by amplified green area (Fig. 2C). It should be noted that BAPTA-AM, an intracellular Ca²⁺ chelator, markedly reversed NNC-55-induced MMP reduction, as evidenced by Fig. 2D. These results indicated that TCC inhibition increased ER-Ca²⁺ release, resulting in interfered ER-Ca²⁺ homeostasis and led to elevated intracellular Ca²⁺ levels in C2C12 myotubes and destruction of cellular organelle structures, which contributed to apoptosis.

TCC inhibition promotes the activation of ERS-related apoptosis in C2C12 myotubes

Given that ERS-mediated ER-Ca²⁺ overload further exacerbates mitochondrial dysfunction and cell apoptosis [30], we detected ERS using ThT, which exhibits fluorescence when it binds to protein aggregates as Daniel described [26]. The results showed that the fluorescence intensity, which represents ERS levels, was significantly enhanced with the increase in NNC-55 concentration in C2C12 myotubes (Fig. 3A,C). The mRNA expression of GRP78 and CHOP also upregulated, which positively correlated with the concentration of NNC-55 (Fig. 3B). TCC inhibition significantly



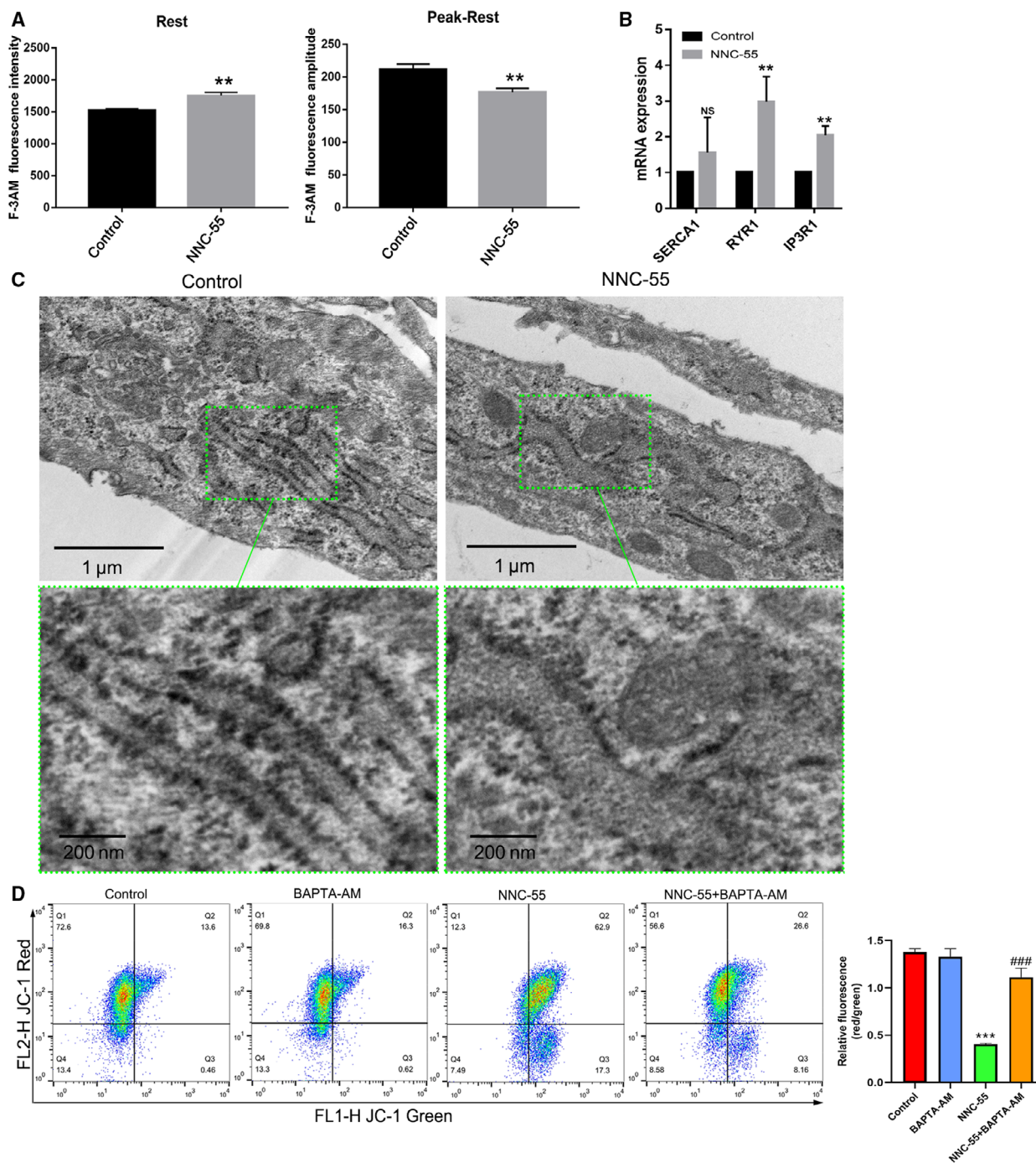


Fig. 2. NNC-55 treatment (10 μM , 24 h) induced ER- Ca^{2+} release and ER- Ca^{2+} dis-homeostasis. (A) To estimate basal Ca^{2+} level, the average Ca^{2+} value for 1 min before stimulation was used. The increment of Ca^{2+} was calculated by subtraction of the basal level from each stimulus-induced peak Ca^{2+} level (30 mM KCl). To quantify the effect of NNC-55, basal Ca^{2+} level at rest and relative amplitude of Ca^{2+} induced by 30 mM KCl were calculated and the graphs presented the measurement of cytoplasmic Ca^{2+} concentration on a rest status and relative amplitude on a KCl-induced peak-rest status; (B) The gene expression related to important molecular components of the Ca^{2+} handling machinery of the ER (SERCA1, RYR1, IP3R1) by qRT-PCR. (C) Morphological observations of subcellular structure in C2C12 myotubes treated by 10 μM NNC-55 for 24h were obtained through transmission electron microscopy. Green frames indicate representative ultrastructural changes in top panels and were amplified in bottom panels. Scale bar, 1 μm (top panels) and 200 μm (bottom panels). (D) MMP was assessed using JC-1 staining by flow cytometry. JC-1 fluorescence ratios (green/red) were calculated. JC-1 staining showed that 10 μM NNC-55 for 24 downregulated MMP with decreased JC-1 red/green ratio in C2C12 myotubes compared to the control cells. These data are presented as the (mean \pm SD) for three independent experiments. NS, no significance. ** $P < 0.01$ vs Control; *** $P < 0.001$ vs Control; ### $P < 0.01$ vs NNC-55, respectively; One-way ANOVA and Dunnett's test were applied.

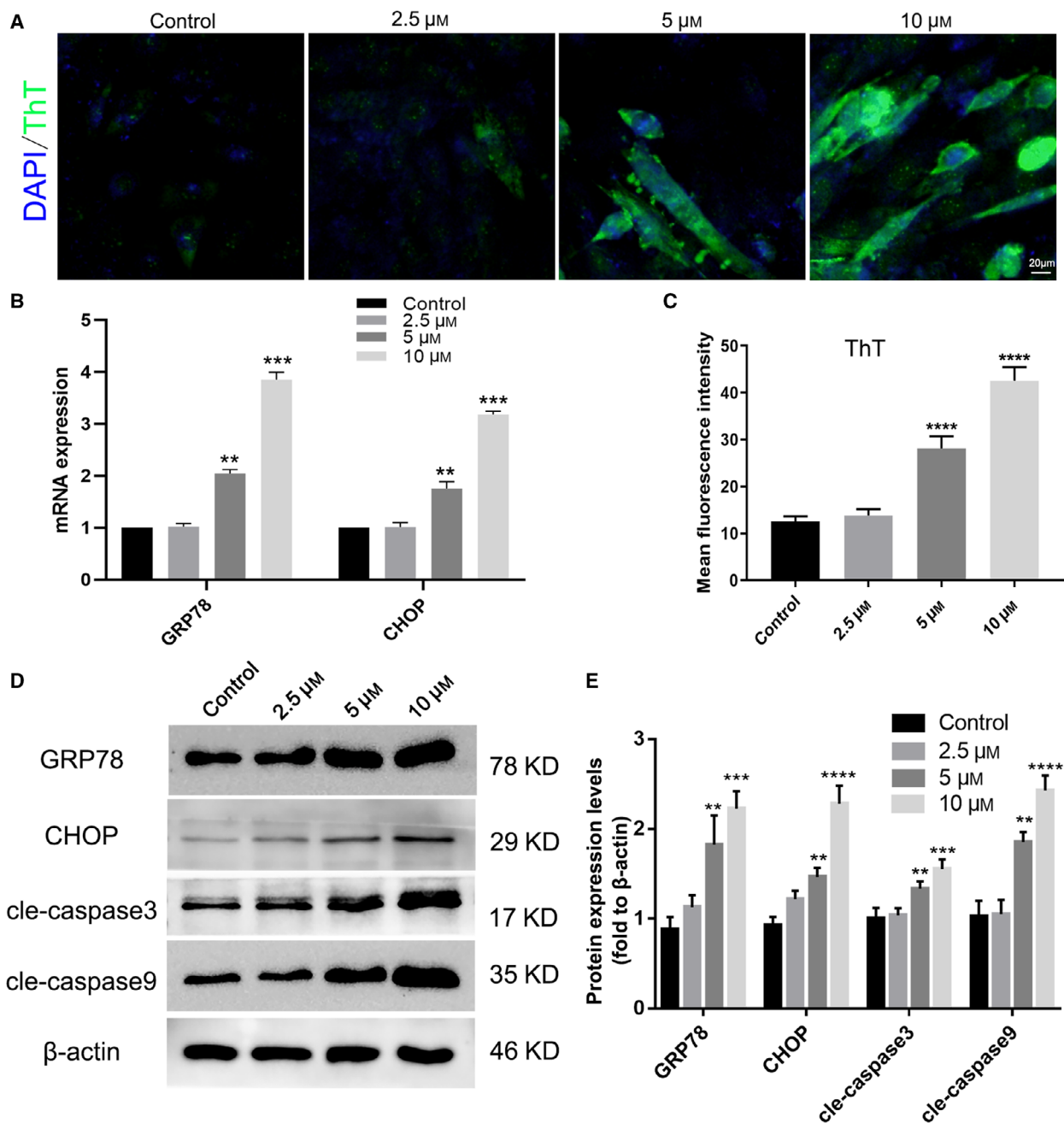


Fig. 3. TCC inhibition induced ERS and increased apoptosis in C2C12 myotubes. C2C12 myotubes were treated with different concentrations of NNC-55 after 4 days of differentiation according to the description in Fig. 1. (A) The intracellular ERS analysis by ThT assay under a fluorescence microscope and mean ThT fluorescence intensities were presented (C); ThT stained green and DAPI stained blue; scale bar, 20 μm ; (B) mRNA expression of ERS-involved genes including GRP78 and CHOP by qRT-PCR analysis in C2C12 myotubes. (D) Protein levels of GRP78, CHOP, cleaved-caspase 3, and cleaved-caspase 9 were analyzed by western blot and quantitation of proteins (E). These data are presented as the (mean \pm SD) for three independent experiments. ** $P < 0.01$, *** $P < 0.001$, **** $P < 0.0001$ vs Control, respectively. Data were analyzed using one-way ANOVA and Dunnett's test.

upregulated the expression of ERS activation-related proteins (GRP78 and CHOP) and apoptosis-related proteins (cleaved caspase 3 and cleaved caspase 9) in a

concentration-dependent manner (Fig. 3D,E). Together, these results indicated that TCC inhibition promoted the activation of ERS and apoptosis in C2C12 myotubes.

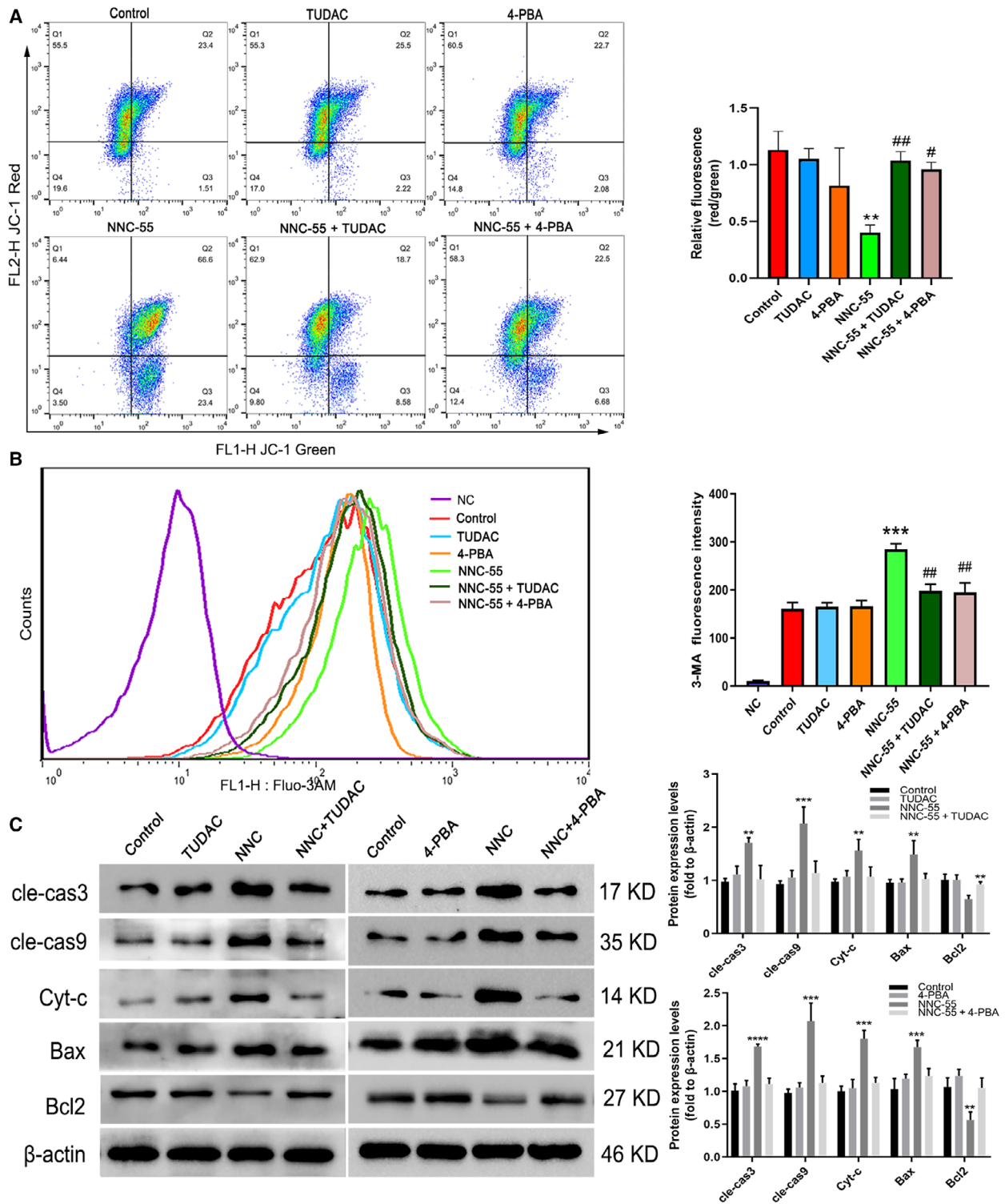


Fig. 4. ERS inhibitors alleviated the promotion of apoptosis and cytoplasmic Ca²⁺ levels of C2C12 myotubes. After differentiated for 4 days, C2C12 myotubes were treated with different single-time drug interventions for 24 h. (A) Measurements of JC-1 red and green fluorescence were performed as described in Fig. 1. (B) Cytoplasmic Ca²⁺ concentration detection on rest status; (C) the protein expression and quantification of different intervention. These data are presented as the (mean ± SD) for three independent experiments. ***P* < 0.01 vs Control; ****P* < 0.001 vs Control; *****P* < 0.001 vs Control; #*P* < 0.05, ##*P* < 0.01 vs NNC-55. Data were analyzed using one-way ANOVA and Dunnett's test.

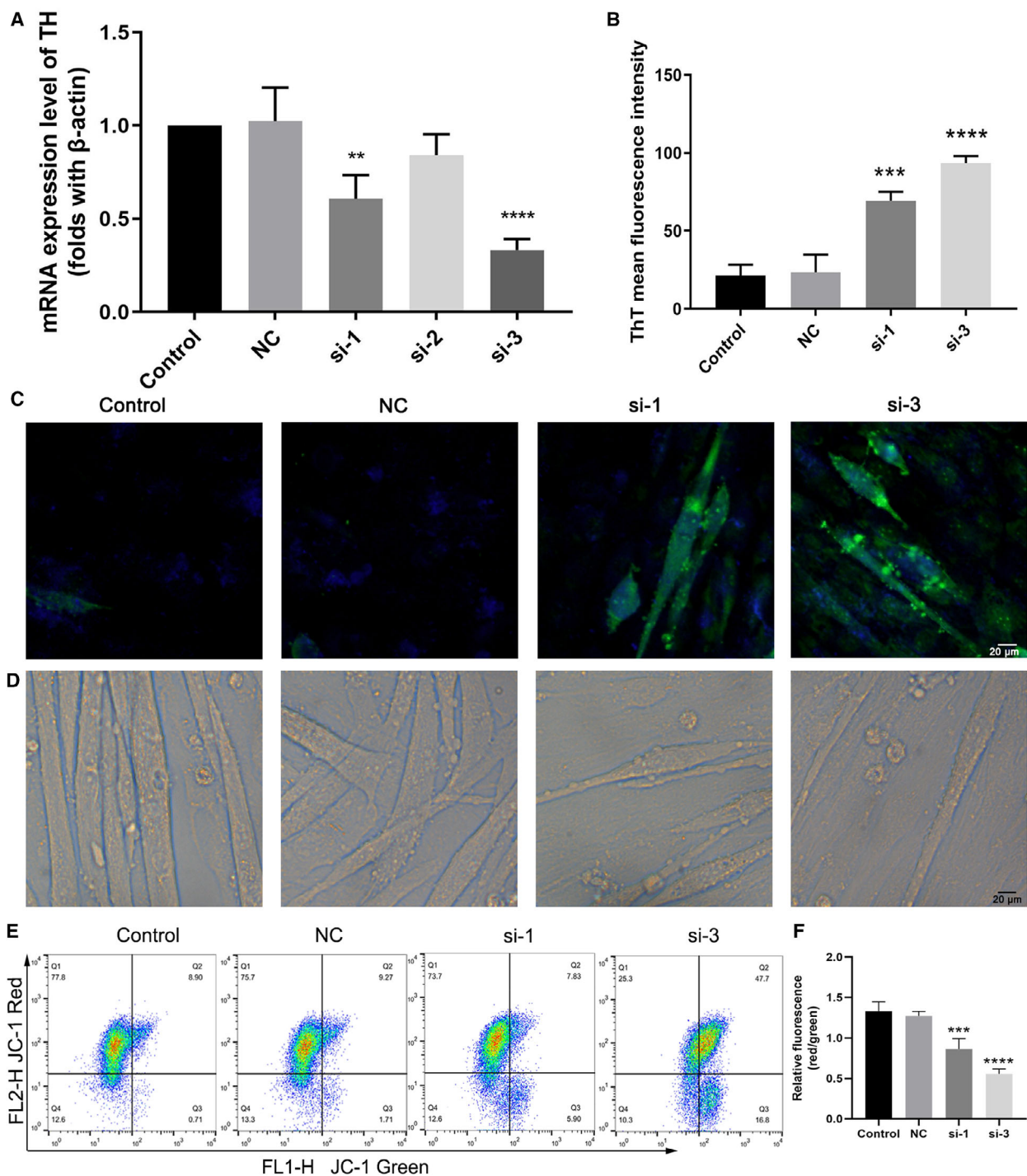


Fig. 5. TH knockdown induced elevated ERS and apoptosis in C2C12 myotubes. (A) qRT-PCR analysis of TH mRNA expression after TH silencing treatment for 48 h. (B, C) Representative ThT (green) fluorescence microscopic images and quantification, showing the ERS levels in myotubes. (D) Representative photographs of morphological changes of C2C12 myotubes; (E, F) MMP analysis using JC-1 staining by flow cytometry and the relative fluorescence quantification of the JC-1 red:JC-1 green ratio as described in Fig. 1. These data are presented as the (mean \pm SD) for three independent experiments. ** $P < 0.01$, *** $P < 0.001$, **** $P < 0.0001$ vs Control. Data were analyzed using one-way ANOVA and Dunnett's test.

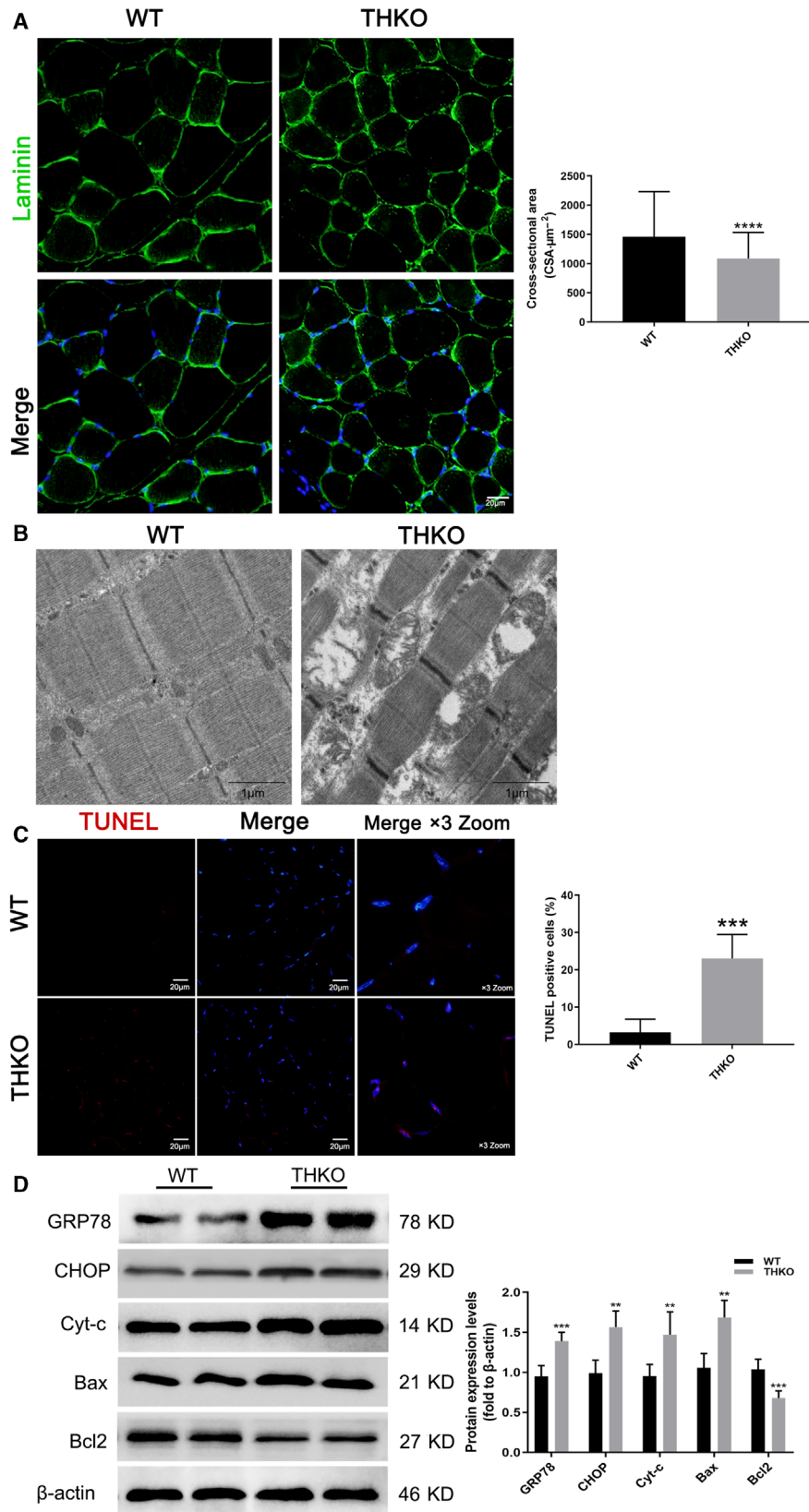


Fig. 6. THKO mice displayed smaller muscle fiber size and ERS-related apoptosis levels in TA. (A) CSA of TA muscle using laminin (green) and merged DAPI (blue) staining, and the quantification. Scale bar, 20 μm ; (B) the ultrastructural morphology observation by a transmission electron microscope. Scale bars, 1 μm . (C) Cell apoptosis in TA muscle tissue by TUNEL assay. TUNEL-positive cells were stained red, and cell nuclei were stained blue by DAPI. Scale bars, 20 μm ; the merged images were amplified three times; (D) western blot results for GRP78, CHOP, Cyt-c, Bax, and Bcl2 expression. These data are presented as the (mean \pm SD) for three independent experiments. $**P < 0.01$, $***P < 0.001$, $****P < 0.0001$ vs Control by Student's *t*-tests (unpaired two-tailed).

ERS inhibitors attenuate the promotion of apoptosis and intracellular Ca^{2+} levels induced by NNC-55

To further investigate the contribution of ERS to mitochondria-related apoptosis induced by NNC-55 treatment, we reduced ERS with two ERS inhibitors, 4PBA [31] and TUDAC [30]. Interestingly, ERS inhibitors attenuated the promotion of MMP reduction induced by NNC-55 (Fig. 4A). Moreover, the fluorescence intensity of intracellular Ca^{2+} staining by Fluo-3 AM was significantly weakened with ERS inhibitor treatment, as shown in the two corresponding curves (Fig. 4B). The protein expression levels of cleaved caspase 3, cleaved caspase 9, Cyt-c, and Bax were also downregulated after ERS inhibitor treatment; in particular, the antiapoptosis protein Bcl2 was significantly upregulated (Fig. 4C). The ERS inhibitors simultaneously attenuated the promotion of both mitochondria-related apoptosis and intensity of Ca^{2+} in C2C12 myotubes induced by NNC-55, suggesting a pathological mechanism in which apoptosis of C2C12 myotubes induced by TCC inhibition is ERS-related.

TH knockdown by siRNAs potentiates ERS and apoptosis in C2C12 myotubes

To further verify the ERS-related pro-apoptotic effect of the TCC inhibitor on C2C12 myotubes, we generated TH knockdown C2C12 cells with three siRNAs. The expression of TH mRNA was mostly downregulated in the si-1 and si-3 groups (with a higher efficiency of TH silencing in the si-3 group) compared to those of the control and NC groups (Fig. 5A). Consistent with the dose-dependent effect of NNC-55 treatment, we also found higher levels of ERS (Fig. 5B,C) and mitochondria-related apoptosis in si-3 group. The morphology of TH-silenced C2C12 myotubes showed more surface blebs and decreased myotube fusion in the si-1 and si-3 groups (Fig. 5D). In addition, a significant decrease of MMP was found in the si-1 and si-3 group (Fig. 5E,F). These results further verified that TCC blockade caused by TH knockdown has a significant effect on ERS activation

and promoting mitochondria-related apoptosis in C2C12 myotubes.

TH knockout mice display muscle wasting with reduced skeletal muscle fiber size and increased ERS-related apoptosis levels

As a proof-of-principle, we then sought to validate the physiological relevance of TCC blockade to skeletal muscle mass and its associated signaling molecule(s) related to apoptosis *in vivo*. To address this, we subjected TA muscles from wild-type (WT) and THKO mice to immunoblotting and ultra-microstructure analyses. Although we did not find an abnormal phenotype in myogenic development, THKO mice displayed muscle wasting. As quantified by CSA, THKO mice displayed a smaller muscle fiber size (Fig. 6A). In addition, THKO muscle sections showed major ultrastructural defects, including loosely packed and disrupted muscle bundles, impaired ER with degranulation in cisternae, as well as swollen mitochondria, whereas WT samples exhibited normal ultrastructure and a tidal structure in the SR zone (Fig. 6B). Furthermore, the percentage of red TUNEL-positive cells was significantly increased in the THKO muscles, indicating significantly elevated apoptosis in THKO muscle (Fig. 6C). Accordingly, THKO muscles showed a uniform increase in the expression of both ERS-related (GRP78 and CHOP) and apoptotic proteins (Cyt-c and Bax), along with significant downregulation of an antiapoptotic protein (Bcl2; Fig. 6D). Together, we concluded that TCC blockade significantly contributes to the occurrence of ERS and apoptosis in skeletal muscle, which is proposed to be one of the mechanisms underlying muscle wasting.

Discussion

Skeletal muscle is a highly dynamic tissue and undergoes continuous remodeling that is responsible for cellular stress. Loss of muscle mass can be the consequence of pathological changes, as observed in muscular dystrophies; the chronic muscle disuse that accompanies aging or muscle-wasting diseases provokes a decline in

mitochondrial content and function, which elicits excessive ROS formation and apoptotic signaling [32]. ER proteostasis surveillance mediated by ERS also plays a crucial physiological role in the maintenance of skeletal muscle and is emerging as a possible driver of cell apoptosis. Our previous study uncovered that TCC inhibition induced C2C12 myotube atrophy through ERS activation and autophagy flux blockade [24]. ERS is upstream of autophagy blockade induced by NNC-55, and mitochondrial dysfunction could also regulate autophagic process through ROS production and mitochondria-specific proteins. Therefore, we further explored the effects of TCC function loss on mitochondria-related apoptosis which may be a trigger of autophagy regulation. Here, we confirmed a novel mechanism that TCC blockade resulted in the occurrence of ERS through CHOP-mediated impingement on the regulation of mitochondria-related apoptosis, which may be involved in the development of muscle wasting.

T-type calcium channel, which is activated by low voltage, is expressed ubiquitously in multiple cell types and organs and mediates intracellular Ca^{2+} signal transduction [23]. As aged skeletal muscle and aged SCs showed decreased amplitude of T-type Ca^{2+} currents [19], it can be speculated that TCCs may alter or blockade with aging. In addition, as an aging-specific response of age-related declines in muscle mass (sarcopenia) [14], the activation of ERS signal cascades has been observed in skeletal muscle in multiple muscle-wasting conditions with GRP78 upregulated. ERS is stimulated by a wide range of cellular environments and events, including increased levels of protein synthesis, an excess or limitation of nutrients, inflammatory challenges, and dysregulated Ca^{2+} levels [9]. Accordingly, we hypothesized that TCC blockade acts as one of the triggers that alters ER homeostasis and initiates the activation of GRP78. We found that the TCC inhibition induced apoptosis and promotes ERS in C2C12 myotubes in a dose-dependent manner and THKO muscle displayed muscle wasting with smaller myofiber size (Fig. 6A). These results suggested effects of apoptotic cell death and ERS induction by TCC blockade.

Considering that ERS-mediated ER Ca^{2+} overload further exacerbates mitochondrial dysfunction and cell apoptosis [30], a possible explanation for why C2C12 apoptosis increased after TCC inhibition may be ERS-mediated reduction in ER Ca^{2+} storage levels. The maintenance of internal Ca^{2+} homeostasis is an essential feature of the proper structure and physiological function of skeletal muscle and is critically required for maintaining homeostatic conditions and structural integrity in the ER/SR zone [18]. Thus, in addition to ER impairments characterized as obvious

degranulation and dilation in cisternae in the ER zone (Fig. 3B), We found that TCC inhibition induced interfered ER- Ca^{2+} homeostasis (Fig. 2B) and increased intracellular Ca^{2+} levels. As a proof, intracellular Ca^{2+} chelator markedly reversed NNC-55-induced apoptosis and ERS inhibitors attenuated the promotion of both apoptosis and intracellular Ca^{2+} levels (Fig. 2C). Since persistent ERS induces downregulation of total and ER- Ca^{2+} stores, it has been reported that ERS increases mitochondrial Ca^{2+} uptake and ROS production, which contributes to decreased mitochondrial transmembrane potential ($\Delta\Psi_m$) [28,31,33,34] and promotes cell survival or cell death. It is reasonable that the close distance associated with the flux of Ca^{2+} between the ER and mitochondria may couple with increased Ca^{2+} uptake by mitochondria at MCSs. These data suggest that apoptosis induction is associated with ERS-related ER- Ca^{2+} dis-homeostasis.

It has been confirmed that CHOP is controlled by the PERK-ATF4 axis when ERS sensors are activated under certain conditions, which induces the expression of proapoptotic genes [12]. CHOP has also been shown to induce apoptosis through the core mitochondrial apoptosis pathway, which is regulated by members of the B cell lymphoma 2 family (i.e., Bax and Bcl2) and ultimately leads to caspase activation [8,35]. Consistent with this, our data showed increased percentage of red TUNEL-positive cells and a significant upregulation of GRP78, CHOP, Cyt-c, and Bax and downregulation of Bcl2 in THKO muscle (Fig. 6D). These results can be explained by the mechanism of which TCC blockade resulted in the occurrence of ERS through CHOP-mediated signal pathway. However, more further studies on detailed intermolecular pathways are required to clarify the role of TCC blockade in skeletal muscle.

In conclusion, our data highlight the mechanism by which TCC blockade induces the occurrence of ERS through CHOP-mediated impingement on the regulation of mitochondria-related apoptosis. ERS-induced ER Ca^{2+} disorders and increased intracellular Ca^{2+} levels contribute to ER impairments and proapoptotic gene expression, which may be involved in the development of skeletal muscle wasting.

Acknowledgements

This work was financially supported through grants from the National Natural Science Foundation of China (grant nos. 81971364 and 81771562), second level fund of the second medical leading talents project of Hubei province (no. [2019]47), special project for Chinese women's pelvic floor dysfunction prevention

and treatment (no. 201817092), and the Fundamental Research Funds for the Central Universities (no. 2042018gf0039).

Conflict of interest

The authors declare no conflict of interest.

Data accessibility

All data used to support the findings of this study are included within the article.

Author contributions

MC and LH conceived and supervised the study; MC and SL designed experiments; MH, JC, and ZZ performed experiments; SH provided new tools and reagents; SH, JM, and JT developed new software and performed simulation studies; MH analyzed data; MC wrote the manuscript; and LH made manuscript revisions. All authors read and approved the final manuscript.

References

- 1 Bohnert KR, McMillan JD and Kumar A (2018) Emerging roles of ER stress and unfolded protein response pathways in skeletal muscle health and disease. *J Cell Physiol* **233**, 67–78.
- 2 Cohen S, Nathan JA and Goldberg AL (2015) Muscle wasting in disease: molecular mechanisms and promising therapies. *Nat Rev Drug Discov* **14**, 58–74.
- 3 Dupont-Versteegden EE (2006) Apoptosis in skeletal muscle and its relevance to atrophy. *World J Gastroenterol* **12**, 7463–7466.
- 4 Bloemberg D and Quadrilatero J (2019) Autophagy, apoptosis, and mitochondria: molecular integration and physiological relevance in skeletal muscle. *Am J Physiol Cell Physiol* **317**, C111–C130.
- 5 Cea LA, Puebla C, Cisterna BA, Escamilla R, Vargas AA, Frank M, Martínez-Montero P, Prior C, Molano J, Esteban-Rodríguez I *et al.* (2016) Fast skeletal myofibers of mdx mouse, model of Duchenne muscular dystrophy, express connexin hemichannels that lead to apoptosis. *Cell Mol Life Sci* **73**, 2583–2599.
- 6 Berchtold MW, Brinkmeier H and Muntener M (2000) Calcium ion in skeletal muscle: its crucial role for muscle function, plasticity, and disease. *Physiol Rev* **80**, 1215–1265.
- 7 Stutzmann GE and Mattson MP (2011) Endoplasmic reticulum Ca(2+) handling in excitable cells in health and disease. *Pharmacol Rev* **63**, 700–727.
- 8 Hetz C (2012) The unfolded protein response: controlling cell fate decisions under ER stress and beyond. *Nat Rev Mol Cell Biol* **13**, 89–102.
- 9 Wang M and Kaufman RJ (2016) Protein misfolding in the endoplasmic reticulum as a conduit to human disease. *Nature* **529**, 326–335.
- 10 Gorman AM, Logue SE, Szegezdi E and Samali A (2006) Mediators of endoplasmic reticulum stress-induced apoptosis. *EMBO Rep* **7**, 880–885.
- 11 Hammadi M, Oulidi A, Gackière F, Katsogiannou M, Slomianny C, Roudbaraki M, Dewailly E, Delcourt P, Lepage G, Lotteau S *et al.* (2013) Modulation of ER stress and apoptosis by endoplasmic reticulum calcium leak via translocon during unfolded protein response: involvement of GRP78. *FASEB J* **27**, 1600–1609.
- 12 Li Y, Guo Y, Tang J, Jiang J and Chen Z (2014) New insights into the roles of CHOP-induced apoptosis in ER stress. *Acta Biochim Biophys Sin (Shanghai)* **46**, 629–640.
- 13 Burman A, Kropski JA, Calvi CL, Serezani AP, Pascoalino BD, Han W, Sherrill T, Gleaves L, Lawson WE, Young LR *et al.* (2018) Localized hypoxia links ER stress to lung fibrosis through induction of C/EBP homologous protein. *JCI Insight* **3**, e99543. doi: [10.1172/jci.insight.99543](https://doi.org/10.1172/jci.insight.99543)
- 14 Ogata T, Machida S, Oishi Y, Higuchi M and Muraoka I (2009) Differential cell death regulation between adult-unloaded and aged rat soleus muscle. *Mech Ageing Dev* **130**, 328–336.
- 15 Ikezoe K, Nakamori M, Furuya H, Arahata H, Kanemoto S, Kimura T, Imaizumi K, Takahashi MP, Sakoda S, Fujii N *et al.* (2007) Endoplasmic reticulum stress in myotonic dystrophy type 1 muscle. *Acta Neuropathol* **114**, 527–535.
- 16 Carter MT, McMillan HJ, Tomin A and Weiss N (2019) Compound heterozygous CACNA1H mutations associated with severe congenital amyotrophy. *Channels (Austin)* **13**, 153–161.
- 17 Pushparaj C, Das A, Purroy R, Nager M, Herreros J, Pamplona R and Canti C (2015) Voltage-gated calcium channel blockers deregulate macroautophagy in cardiomyocytes. *Int J Biochem Cell Biol* **68**, 166–175.
- 18 Berthier C, Monteil A, Lory P and Strube C (2002) α 1H mRNA in single skeletal muscle fibres accounts for T-type calcium current transient expression during fetal development in mice. *J Physiol* **539**, 681–691.
- 19 Luin E and Ruzzier F (2007) The role of L- and T-type Ca²⁺ currents during the *in vitro* aging of murine myogenic (i28) cells in culture. *Cell Calcium* **41**, 479–489.
- 20 Sankhe S, Manousakidi S, Antigny F, Arthur Ataam J, Bentebbal S, Ruchon Y, Lecerf F, Sabourin J, Price L, Fadel E *et al.* (2017) T-type Ca(2+) channels elicit pro-proliferative and anti-apoptotic responses through impaired PP2A/Akt1 signaling in PSMCs from

- patients with pulmonary arterial hypertension. *Biochim Biophys Acta Mol Cell Res* **1864**, 1631–1641.
- 21 Snutch TP and Zamponi GW (2018) Recent advances in the development of T-type calcium channel blockers for pain intervention. *Br J Pharmacol* **175**, 2375–2383.
- 22 Bhargava A and Saha S (2019) T-Type voltage gated calcium channels: a target in breast cancer? *Breast Cancer Res Treat* **173**, 11–21.
- 23 Zamponi GW, Striessnig J, Koschak A and Dolphin AC (2015) The physiology, pathology, and pharmacology of voltage-gated calcium channels and their future therapeutic potential. *Pharmacol Rev* **67**, 821–870.
- 24 Li S, Hao M, Li B, Chen M, Chen J, Tang J, Hong S, Min J, Hu M and Hong L (2020) CACNA1H downregulation induces skeletal muscle atrophy involving endoplasmic reticulum stress activation and autophagy flux blockade. *Cell Death Dis* **11**, 279.
- 25 Fan J, Kou X, Jia S, Yang X, Yang Y and Chen N (2016) Autophagy as a Potential Target for Sarcopenia. *J Cell Physiol* **231**, 1450–1459.
- 26 Beriault DR and Werstuck GH (2013) Detection and quantification of endoplasmic reticulum stress in living cells using the fluorescent compound, Thioflavin T. *Biochim Biophys Acta* **1833**, 2293–2301.
- 27 Salucci S, Battistelli M, Burattini S, Squillace C, Canonico B, Gobbi P, Papa S and Falcieri E (2010) C2C12 myoblast sensitivity to different apoptotic chemical triggers. *Micron* **41**, 966–973.
- 28 Bernhardt ML, Zhang Y, Erxleben CF, Padilla-Banks E, McDonough CE, Miao YL, Armstrong DL and Williams CJ (2015) CaV3.2 T-type channels mediate Ca²⁺(+) entry during oocyte maturation and following fertilization. *J Cell Sci* **128**, 4442–4452.
- 29 Nishizawa Y, Takahashi K, Oguma N, Tominaga M and Ohta T (2018) Possible involvement of transient receptor potential ankyrin 1 in Ca²⁺ signaling via T-type Ca²⁺ channel in mouse sensory neurons. *J Neurosci Res* **96**, 901–910.
- 30 Uppala JK, Gani AR and Ramaiah K (2017) Chemical chaperone, TUDCA unlike PBA, mitigates protein aggregation efficiently and resists ER and non-ER stress induced HepG2 cell death. *Sci Rep* **7**, 3831.
- 31 Lee CS, Hanna AD, Wang H, Dagnino-Acosta A, Joshi AD, Knoblauch M, Xia Y, Georgiou DK, Xu J, Long C *et al.* (2017) A chemical chaperone improves muscle function in mice with a RyR1 mutation. *Nat Commun* **8**, 14659.
- 32 Hood DA, Ugucioni G, Vainshtein A and D'Souza D (2011) Mechanisms of exercise-induced mitochondrial biogenesis in skeletal muscle: implications for health and disease. *Compr Physiol* **1**, 1119–1134.
- 33 Ainbinder A, Boncompagni S, Protasi F and Dirksen RT (2015) Role of Mitofusin-2 in mitochondrial localization and calcium uptake in skeletal muscle. *Cell Calcium* **57**, 14–24.
- 34 Marchi S, Patergnani S, Missiroli S, Morciano G, Rimessi A, Wieckowski MR, Giorgi C and Pinton P (2018) Mitochondrial and endoplasmic reticulum calcium homeostasis and cell death. *Cell Calcium* **69**, 62–72.
- 35 Szegezdi E, Logue SE, Gorman AM and Samali A (2006) Mediators of endoplasmic reticulum stress-induced apoptosis. *EMBO Rep* **7**, 880–885.